Ferrosilicate-based heterogeneous Fenton catalysts: Influence of crystallinity, porosity, and iron speciation

E.V. Parkhomchuk[a,b], J. García-Aguilar[c], K.A. Sashkina[a,b], A. Berenguer-Murcia[c], D. Cazorla-Amorós[c], R.I. Dralyuk[a,b], A.B. Ayupov[a,b], I. Danilova[a]

[a] Boreskov Institute of Catalysis SB RAS, 5 Lavrentieva St., Novosibirsk 630090, Russia.

[b] Novosibirsk State University, 2 Pirogova St., Novosibirsk 630090, Russia.

c Instituto Universitario de Materiales de Alicante y Departamento de Química Inorgánica, Universidad de Alicante, Ctra. San Vicente del Raspeig s/n, Ap. 99, E-03080 Alicante, Spain

E-mail: ekaterina@catalysis.ru

Abstract

Different ferrosilicate samples have been prepared with varying degrees of crystallinity, porous texture, and speciation of the Fe sites by both hydrothermal and sol-gel procedures: Fe-silicalite-1 with microcrystals (2-10 μm) and nanocrystals (180 nm), Fe-containing composite material consisting of silicalite-1 and amorphous silica, and two samples of mesoporous Fe-containing amorphous silica Fe-SiO_2. The resulting solids have been tested for their potential as organic pollutants removal under Fenton-like conditions in heterogeneous catalytic wet peroxide oxidation of phenol and clarithromycin lactobionate. Our results indicate that the three aforementioned parameters show a strong interplay towards the abatement of pollutants in liquid phase. Thus, samples with high crystallinity and sufficient acid character show an improved performance in the oxidation of organic contaminants over amorphous samples in which the Fe speciation is very well controlled.

Keywords: Fe-silicalite-1, Fe-SiO_2, Nanocrystals, Heterogeneous Fenton catalyst, Hydrogen peroxide, phenol oxidation, clarithromycin lactobionate.

Introduction

The removal of organic contaminants from both gas and aqueous phase is an ever growing need due to stricter environmental regulations [1]. In this respect, phenol and phenol-derived compounds constitute a highly relevant family of compounds which are present in many industrial effluents [2,3]. Phenol concentrations over 1 $mg \cdot L^{-1}$ already endarger aquatic life, and thus the Environmental Protection Agency of America has fixed the limit at 1 ppb and 100 ppb in surface and nonchlorinated water, respectively [4]. On average, phenol and phenol-derived compounds are stable and highly toxic, which makes their removal both difficult and necessary. In order to alleviate this situation, physical, chemical, and biological technologies (and their

combinations) have been investigated to remove phenols from liquid effluents, being phenol most often used as model compound in order to explore suitable removal technologies [5,6,7].

It is in this context that Advanced Oxidation Processes (AOPs) are nowadays considered to be one of the most effective methods to remove organic contaminants. Fenton and photo-Fenton oxidation are two AOPs showing the greatest potential [8,9]. Given the disadvantages Fenton and photo-Fenton processes show under homogeneous media, their application prospects have been severely limited. Thus, significant efforts have been made to develop different heterogeneous Fenton-like catalysts [10,11,12,13,14].

As Cano-Casanova *et al*. have reported recently for a related photocatalytic reaction (the removal of propene at low concentrations using TiO_2-based materials) [15], several factors need to be weighed in whenever selecting a suitable solid for organic pollutant removal processes, such as sample crystallinity, presence of different crystal phases, and surface chemistry of the (photo)catalysts. When catalytically active species different from those present in the bulk solid are needed, their incorporation into the solid framework (or not) as well as their speciation play a key role. We reported recently how iron speciation into silica-based materials (both during and post-synthesis) is determinant in their catalytic activity [16,17]. For example, earlier we have shown that Fe-ZSM-5 is effective heterogeneous Fenton catalyst in total hydrogen peroxide oxidation of a series of organic substrates with low molecular weight (MW) [18] and ineffective in oxidation of high MW substances because of the specific porous structure of zeolites [19]. This is due to excessive distance from catalytic sites where the hydroxyl radicals are formed inside the zeolite crystal to the organic molecule adsorbed on the external surface of crystal particle. These diffusion limitations result in prevalence of oxygen release reaction over organic molecule oxidation process in case of high MW substrates. It was shown that the problem of diffusional limitations may be solved by using hierarchically porous zeolitic material, the activity of hierarchical Fe-ZSM-5 appeared to be really improved in the oxidation of large Na_2EDTA molecule and high MW lignin compared with a conventional zeolite [20]. On the other hand not only the distance from catalytic sites to the organic substrate is important, but also the particle size and crystallinity of the matrices in which the iron species are located seems to be also substantial. In this respect, the catalytic activity of ferric species in hydrogen peroxide decomposition for small 330-nm crystals of Fe-ZSM-5 was 1.4 times higher than for large zeolite crystals, and a significant decrease of the activity was observed for samples containing amorphous silica phase [21]. In some works iron species supported in amorphous silica matrices, including highly ordered mesoporous ones, have been shown to be promising heterogeneous Fenton or photo-Fenton catalysts, the iron loading in the support being more than

15 wt.% [22,23,24]. There are several strategies which allow tuning all the aforementioned parameters with relative ease, and among those there are two which are very widespread thanks to their simplicity and reproducibility: hydrothermal synthesis and sol-gel synthesis. The former allows the obtention of crystalline phases with high quality which can furthermore be adapted to tune the crystallite size and even incorporate heteroatoms at given crystal locations. The latter can give rise to crystalline solids under the appropriate working conditions, but what is perhaps most interesting about it is the possibility to tune the structure of the resulting solids in different length scales as well as incorporate heteroatomic species at the desired locations if the hydrolysis of the precursor salts is controlled properly [16].

In order to develop suitable heterogenous catalysts which work under Fenton conditions in liquid phase, in this study we have prepared a series of silica-based materials doped with less than 1wt.% of iron following either hydrothermal or sol-gel routes. Through these approaches we have modified the crystallinity, porous texture, and iron speciation to come up with a series of solids to be used in the wet peroxide oxidation of a small molecule – phenol- , and a large molecule – clarithromycin lactobionate (CL). Our results indicate that while micropores do not play a significant role in the removal of these contaminants, the interplay between external surface area and acidity seem to be the combination which renders the best pollutant abatement results.

Experimental

1.1. Materials

Tetrapropylammonium hydroxide (TPAOH, 25 wt. % solution in water, Acros), tetrapropylammonium bromide (TPABr, 98 %, Aldrich), tetraethylorthosilicate (TEOS, ≥98%, Angara-reactive, silica (fumed, ≥99 %, Aldrich), ethanol (EtOH, 95%, Pharmaceya) and $Fe(NO_3)_3 \cdot 9H_2O$ (≥99%, Merck) were used for Fe-silicalite-1 micro- and nanocrystals preparation. Styrene monomer (Angara-reactive, inhibited with 1% hydroquinone), sodium hydroxide (NaOH, 98%, Tellura) and potassium persulfate (≥99%, Acros) were used for obtaining latex which was used in preparation of Fe-composite and Fe-SiO_2 sample 1. A tri-block copolymer (Pluronic® F127, BASF), urea, acetic acid (0.01M solution), $Fe(NO_3)_3 \cdot 9H_2O$ and Tetramethyl orthosilicate (TMOS) were used for Fe-SiO_2 sample 2 preparation. Oxalic acid ($H_2C_2O_4 \cdot 2H_2O$, Reakhim) was used for transforming Fe-silicalite-1 microcrystals into protonic state. Hydrogen peroxide (H_2O_2, 30 %, Baza No.1 Khimreaktivov), phenol (Reakhim), clarithromycin lactobionate (CL, Abbott Laboratories) were applied for catalytic experiments.

1.2. Synthesis of Fe-silicalite-1

The synthesis of Fe-silicalite-1 microcrystals was performed using the following chemical composition of the precursor solution: 1.00 SiO_2 : 0.1 Na_2O : 0.11 TPABr : 0.006 Fe_2O_3 : 33 H_2O. In a typical synthesis procedure, 40 g of silica was gradually added to 400 mL of an aqueous solution containing 5.36 g NaOH and 19.5 g of TPABr under magnetic stirring at ambient temperature. After stirring for 15 min, 3.2 g of $Fe(NO_3)_3 \cdot 9H_2O$ dissolved in 5 ml of distilled water were added dropwise to obtain a milky suspension. After further stirring for 10 min, 100 mL-batches of the gel mixture were transferred to a 150-mL Teflon-lined stainless-steel autoclaves. The autoclave was maintained in an oven at 433 K for 72 h. After the hydrothermal treatment, the solid product was filtered, rinsed with distilled water and dried at 373 K for 12 h. The sample was calcined at 773 K for 5 h and then activated by acid treatment followed by calcination. For the activation, calcined Fe-silicalite-1 was put in 1 M aqueous solution of oxalic acid with the Fe-silicalite-1 concentration of 100 $g \cdot L^{-1}$ and stirred for 30 min at 323 K. The sample after acid treatment was filtered and rinsed with distilled water until pH=7.0, dried in air at 373 K for 12 h and calcined at 773 K for 3 h.

Synthesis of Fe-silicalite-1 nanocrystals was carried out as follows. 120 ml of TEOS diluted with 120 ml of ethanol was added at once to 240 ml of TPAOH (12.5 wt. %) under vigorous stirring for 20 min, then 2.6 g of $Fe(NO_3)_3 \cdot 9H_2O$ dissolved in 5 ml of distilled water was added dropwise. After stirring for 20 min, 100 mL-batches of the resultant clear light-yellow gel with 1.00 SiO_2 : 0.28 TPAOH : 0.006 Fe_2O_3 : 4.79 EtOH : 1.75 H_2O molar composition were placed to 150-mL Teflon-lined stainless steel autoclaves and subjected to hydrothermal treatment in an oven at 363 K for 7 days. The milky suspension produced was purified in a series of three steps consisting of centrifugation at relative acceleration of 3000 g for 5 h, followed by removal of the mother liquor and redispersion in distilled water under ultrasonication. Purified Fe-silicalite-1 was separated by centrifugation, dried at 323 K for 12 h and calcined at 773 K for 5 h.

Fe-silicalite-1 powders were ground in a mortar, and the fraction < 200 μm was separated by sifting for adsorption and catalytic experiments.

1.3. Synthesis of Fe-composite and Fe-SiO_2 sample 1

Fe-composite and Fe-SiO_2 sample 1 were prepared using polystyrene microspheres which were in turn produced via emulsifier-free emulsion polymerization of styrene at 363 K as described earlier [25], using potassium persulphate as initiator. The materials synthesis was as follows. 10.0 g of dried polystyrene (PS) beads were ground in a mortar, washed by ethanol, and dried at room temperature. The obtained PS template was impregnated by $Fe(NO_3)_3$ solution with 0.15 g of the nonahydrate salt in 5 ml of ethanol, dried at 323 K for 1 h and mixing every 10 min. Then for synthesis of Fe-composite the dried mixture was kept over boiling water for 30 min. For synthesis of Fe-SiO_2 sample 1 this procedure was not applied. For both samples PS

template was impregnated with the gel with SiO_2:Fe_2O_3:TPAOH:H_2O molar ratio of 1:0.008:0.51:17.5 with weight ratio 0.13 SiO_2: 1 PS. The mixtures were subjected to hydrothermal synthesis at 383 K for 40 h. The products were washed with abundant amount of water, then dried at an ambient temperature overnight and finally calcined at 773 K for 8 h in air.

1.4. Synthesis of Fe-SiO_2 sample 2

All the ferrosilicate samples referred to as "Fe-SiO_2 sample 2" in this study were prepared as reported in our earlier work [16]. In a representative example the synthetic procedure was conducted as follows, 0.400 g of surfactant (Pluronic® F127, BASF), 0.452 g of urea and 5.052 g of 0.01M acetic acid aqueous solution were added under vigorous stirring in a beaker and kept under stirring for 80 min, the final pH of the resulting solution being around 4. The necessary amount of iron precursor ($Fe(NO_3)_3 \cdot 9H_2O$, 99.99%) was added to the solution and the mixture was stirred for 1 h. The solution was then cooled at 0ºC by means of an ice bath under constant stirring and the silica precursor was added dropwise (2.030 g TMOS). This solution was kept under stirring for 40 min at 273 K.

In order to finalize the sol-gel process, the mixture was introduced in a 50 mL Teflon-lined stainless steel autoclave and heated at 313 K for 20 h in order to age the sol (the pH after this step remained around 4). After this, the sample was submitted to hydrothermal treatment at 393 K for 6 h, causing the urea decomposition (the final pH of the supernatant liquid was around 9-10). The resulting solids were activated by calcination at 823 K for 6 hours (heating rate 10ºC/min) in a muffle furnace in order to remove the surfactant and all unwanted precursors.

1.5.Characterization

Powder X-ray diffraction (XRD) patterns were recorded from a Siemens D500 diffractometer equipped with a Cu Kα radiation (λ = 0.154 nm) for samples Fe-silicalite-1, Fe-composite and Fe-SiO_2 sample 1. The crystal phase composition and crystallinity of Fe-SiO_2 sample 2 were determined by X-ray diffraction (XRD) analysis using a SEIFERT 2002 equipment using Cu Kα radiation. The scanning velocity was 2º/min, and diffraction patterns were recorded in the angular 2θ range of 6–80º. The chemical composition of the samples was determined by X-ray fluorescence spectrometry with Thermo Scientific ARL Perform'X X-Ray fluorescence spectrometer and inductively coupled plasma optical emission spectrometry (ICP-OES). X-ray photoelectron spectroscopy (XPS) spectra were recorded by an instrument SPECS Surface Nano Analysis GmbH, supplied with semi-spherical analyzer PHOIBOS-150, 9-channel electron detector and XR-50 emitter with double Al/Mg anode. Experiments were carried out with Al Kα ($h\nu$ = 1486.6 eV), irradiation and energy calibration was performed by Si2p signal with the internal

standard method. Scanning electron microscopy (SEM) images were taken with a JEOL JSM-6460LV microscope at an operating voltage of 15-20 kV.

Textural characteristics of the samples were evaluated using nitrogen adsorption at 77K. The isotherms were measured by means of a QUADRASORB evo adsorption analyzer (Quantachrome Instruments, USA). Prior to measurements, all samples were outgassed at 623 K for 5 h. Surface areas were calculated using BET method based on the IUPAC recommendations [26]. Micropore volume and external surface area (the specific area outside micropores) were estimated using α_s-plot method [27]. Pore size distribution for pores higher than 2nm was computed by BJH method applied to adsorption branch of the isotherms as recommended by Rouquerol [27] using the software supplied along with the instrument.

The structure properties of the samples were analyzed by Infrared spectrometry using KBr pellet technique (a typical pellet containing 1 wt% of a sample). IR spectra were recorded on a Shimadzu FTIR-8300 spectrometer within the spectral range of 350–4000 cm^{-1} with a resolution of 4 cm^{-1}.

1.6.Adsorption and catalytic experiments

Phenol adsorption experiments were carried out at room temperature (293-298 K) for 1 h using m_{cat} = 0.2 g: The solution volume was 10 mL. Catalytic oxidation of phenol and CL by hydrogen peroxide was carried out in a 50 mL thermostatted glass batch reactor agitated with a magnetic stirrer. In the experiments using phenol, the volume of the liquid phase was 11 mL, catalyst concentration – 20 $g \cdot L^{-1}$, T = 303 K, initial concentration of H_2O_2 was 1 M and phenol − 0.5 $g \cdot L^{-1}$. In the experiments on CL, the volume of the liquid phase was 20 mL, catalyst concentration – 20 $g \cdot L^{-1}$, T = 313 K, initial concentration of H_2O_2 was 1.5 M and CL − 0.3 $g \cdot L^{-1}$. We measured the kinetic curves of CO_2 and O_2 emission with a mass spectrometer HiCube RGA100. Before the hydrogen peroxide addition, the suspension of the catalyst and phenol or CL was kept with stirring for 60 or 30 min, respectively.

Results and discussion

According to XRD analyses (Fig. 1 SI) phase composition of Fe-silicalite-1 microcrystals and nanocrystals corresponds to MFI structure [28], while both Fe-SiO_2 samples are totally amorphous. Crystallinity was evaluated from reflexes area at 22–25° with relation to the most crystallized sample – Fe-silicalite-1 nanocrystals. 58% of Fe-composite is crystallized to MFI phase (Table 1) [29].

The IR skeletal spectra of the samples are reported in Fig. 1. The very strong band centered at 1105 cm^{-1}, with an additional weak peak at 1230 cm^{-1}, is assigned to the Si–O–Si asymmetric stretching mode (ν^{as}, inner SiO_4 tetrahedron). The weaker band at 805 cm^{-1} is due to

the corresponding Si–O–Si symmetric stretching mode (ν^s, outer SiO_4 tetrahedron), that has also a Si–O–Si in plane bending character, while the strong band at 453 cm^{-1} is associated to the Si–O–Si rocking mode (out-of-plane bending). These features are present in silica-containing materials such as different types of zeolites, silica and quartz [30,31]. The weaker features in the region 700–500 cm^{-1} and the quite strong band at 550-562 cm^{-1} are attributed to double rings of tetrahedra in zeolitic framework and it is not observed in amorphous silica [31, 32]. The intensity value of the last characteristic band gives an approximate estimation of the crystallinity (Table 1). It should be noted that both Fe-SiO_2 samples 1 and 2 give no reflections on XRD and Fe-SiO_2 sample 1 shows 6% crystallinity according to IR, meaning that the sample contains very small crystallites. Estimation of crystallinity for Fe-silicalite-1 microcrystals by IR method should be considered with caution, since chemical composition of the material is quite different with relation to the others (Table 2), as well as the composition of the initial gel for crystallization being different from that of the other samples.

The splitting of the band around 1105 cm^{-1} with the formation of a band at 1032 cm^{-1}, observed here for Fe-silicalite-1 microcrystals, has been firstly reported by T. Armaroli et al. for large crystals of ZSM-5 zeolite [30]. The phenomenon was attributed to the TO–LO (transverse-longitudinal optical mode) splitting due to the elliptical shape of the big particle samples, which cannot be observed on the small particle sample [30]. Fe-silicalite-1 microcrystals actually represent polycrystals of 2-10 μm in diameter, but spherical rather than elliptical (Fig. 2), and the splitting is probably associated to the difference between bulk and surface Si-O-Si modes. The splitting is also independent from Si/Al ratio (Table 2). The sample Fe-silicalite-1 nanocrystals represents uniform small particles with 180 nm in diameter (Fig. 2) and shows a narrow IR absorption band at 1105 cm^{-1} without splitting. Fe-SiO_2 sample 1 represents large aggregates, consisting of silica globules with wide particle size distribution, while Fe-SiO_2 sample 2 is more uniform in aggregates and globules size (Fig. 2). IR spectra of both Fe-SiO_2 samples show a lower energy shoulder of the band at 1105 cm^{-1}. Fe-composite consists of globules, both silicalite-1 crystals and amorphous silica, with particle size no more than 200 nm (Fig. 2) and the spectrum is a superposition of Fe-SiO_2 sample 1 and Fe-silicalite-1 nanocrystals spectra (Fig. 1). According to IR analyses there are no absorption bands corresponding to Fe_2O_3 phase which may be due to low iron content in all samples.

X-ray photoelectron spectroscopy (XPS) analyses show that iron ions are in trivalent state in all samples – the binding energies for Fe2$p_{3/2}$ in the samples are from 711.3 to 712.1 eV (Table 1 SI), admixtures such as K and Na are also observed (Table 2 SI). Near-surface layer of Fe-composite is enriched by iron ions compared with that one of other samples (Table 2 SI). Fe_2O_3 phase is not registered also by XPS – only one O*1s* peak is observed for all samples at

532.6-532.7 eV, while there is no peak at 529 eV, corresponding to oxygen in Fe_2O_3 phase (Fig. 3b SI) [33]. However according to UV-Vis DR data, two samples, namely Fe-composite and Fe-SiO_2 sample 1, contain clusters of iron ions – the samples exhibit a shoulder around 20,000 cm^{-1}, which is due to an asymmetric peak of large iron oxide aggregates. A band around 27,600 cm^{-1}, which is also due to large iron oxide clusters. This band was proposed by Hensen et al to relate to iron in γ-FeOOH species [34], but our thermodynamic calculation showed that the most favorable state of clusters in this case are goethite (α-FeOOH) or hematite (α-Fe_2O_3) [35]. The intense band at 39,000 cm^{-1} in the spectra of Fe-silicalite-1 microcrystals and Fe-SiO_2 sample 2 points to the presence of small clusters of Fe^{3+}. The shoulder at 35000 cm^{-1} for all samples may be ascribed to the metal–oxygen charge transfer in the clusters of iron in octahedral oxygen coordination. Earlier we have shown that large iron oxide clusters are not active in heterogeneous Fenton reactions, and two samples: Fe-composite and Fe-SiO_2 sample 1, containing them, are expected to have poor catalytic activity in wet hydrogen peroxide oxidation of organic compounds.

Fig.4 depicts that nitrogen adsorption on silicalite-based samples at 77 K can be described by Type I isotherms usual for microporous samples with additional features of mesopores. The isotherms of nitrogen adsorption on amorphous silica samples at 77 K demonstrate Type IV isotherms usual for mesoporous samples. In all isotherms the hysteresis loop is rather narrow making the denomination of the hysteresis type not straightforward. To avoid the nitrogen adsorption artifact due to the steep desorption at p/p_0 of 0.4-0.5 we used adsorption branch of isotherm to calculate pore size distribution for pores larger than 2 nm [27]. Table 1 gives textural characteristics of the samples under study. Fig. 5 illustrates cumulative (integral) pore size distribution computed by BJH method. Fe-SiO_2 samples demonstrate the higher total pore volume than that of Fe-silicalite-1 samples and the virtual lack of micropores, where Fe-SiO_2 sample 2 has more narrow size distribution (one can see the visible step on pore size distribution) and equal total pore volume comparable to that of Fe-SiO_2 sample 1. Between microporous samples, Fe-composite shows the highest total pore volume and the widest pore size distribution in mesopore range without any definite pore size. Fe-silicalite-1 nanocrystals and microcrystals show the step on pore size distribution near 50 nm of pore size diameter, but the former has six times higher mesopore volume. Mesoporosity of Fe-SiO_2 sample 2 is most likely formed by monodispersed particles of SiO_2 with a size smaller than nanocrystals of Fe-silicalite-1, which results in a lower mesopores size – near 10 nm, that correlates well with electron microscopy data.

These properties (phase, textural and chemical) have the key effect on adsorption of phenol. Fig. 6 shows isotherms of phenol adsorption on all samples at room temperature, the

resulting adsorption characteristics being presented in Table 3. Adsorption of phenol is monolayer on silicalite-1 samples and multilayer on amorphous ones – taking into account that the phenol molecule occupies the site of 0,45 nm^2 [36], the theoretical ratio of adsorbed phenol area to S_{BET} is near 36% and more than 100% for crystallized and amorphous samples, respectively. A significant difference in the values of adsorption on crystalline and amorphous samples is mainly due to the surface defectiveness, which is higher for amorphous materials. A similar phenomenon is observed with the better dissolution of amorphous silica in comparison with the crystalline one. Note that experimental ratio of S_{PhOH} to S_{BET} is more than 100% for Fe-composite, containing amorphous phase, and Fe-SiO_2 sample 1, but it is only 56% for Fe-SiO_2 sample 2. This fact may be explained by the difference in acidity of the samples - Fe-SiO_2 sample 2 is more acidic than Fe-SiO_2 sample 1 according to TPD of NH_3 (Table 2). Phenol is a weak acid and the higher the acidity of the sample the less favorable is an interaction between phenol and the surface, and the less favorable is the reaction between ferric sites and phenol with the formation of iron-phenolate complexes. In homogeneous media the formation of $[Fe(C_6H_5OH)_6]^{3+}$ is possible, in heterogeneous system PhOH:Fe should be lower, since not all the valences of ferric cations are free, also iron atoms are in clusters and part of them may be inaccessible for phenol molecules. Nevertheless we observed the PhOH:Fe ratio from 1.5 to 6, being the lowest for Fe-silicalite-1 microcrystals – the most acidic sample-, and the highest for amorphous Fe-SiO_2 sample 2 with moderate acidity among the samples and the lowest iron content. The difference in adsorption constants for microcrystals and nanocrystals of Fe-silicalite-1 may be explained either by acidity or by mesoporosity difference, the contribution and interference of these parameters is still in question.

All samples were tested in the oxidation of phenol by hydrogen peroxide with registration of CO_2 and O_2 evolving during the process (Fig. 7). Phenol mineralization in the presence of crystallized samples of Fe-silicalite-1 is higher than that of amorphous Fe-SiO_2, mainly due to less favorable formation of complexes between oxidation intermediate products and iron cations and lower inhibition effect of intermediates on the catalytic activity. Note that amorphous Fe-SiO_2 sample 2 shows the highest initial oxidation rate but rapidly loses the activity due to fast complexation of iron ions by intermediates. This inhibition effect is clearly seen for three samples, all of them containing amorphous phase: Fe-composite, Fe-SiO_2 sample 1 and Fe-SiO_2 sample 2 – phenol mineralization is not higher than 10% even after 3 hours of the reaction while the oxidant consumption is low (Table 4). Unlike the amorphous samples, crystallized catalysts show a significantly higher mineralization of phenol, the inhibition effect being less pronounced but nonetheless observed – it is 20 and 29% with only 21 and 56 % oxidant consumption over micro- and nanocrystals, respectively. It should be noted that a long initial induction period is

observed for phenol oxidation over the samples (Fig. 7) produced with the use of polystyrene templates, that may be explained by the presence of sulphur-containing species on the surface of the materials, originated from potassium persulphate – the initiator of styrene polymerization. The higher mineralization of phenol for nanocrystals compared with microcrystals of Fe-silicalite-1 may be explained by both higher activity in H_2O_2 decomposition (Fig. 7) and better accessibility of phenol molecules for active oxidative particles due to developed external surface of the first material.

The effect of surface accessibility on catalytic activity of nano- and microcrystals of Fe-silicalite-1 becomes more visible in oxidation of large organic molecule –clarithromycin lactobionate (CL) (Fig. 7). In two hours of the reaction, mineralization of CL over nanocrystals is twice higher than that of for microcrystals. Unlike phenol oxidation, there is no inhibition effect of intermediates on the catalytic activity in CL oxidation by H_2O_2 probably due the absence of iron complexing agents among them. In the presence of crystallized samples the reaction stops as a result of total H_2O_2 consumption with twentyfold excess of the oxidant quantity consumed with relation to stoichiometric one (Table 4). It should be noted that catalytic activity of amorphous Fe-SiO_2 sample 2 is lower compared with crystallized samples in both reactions: H_2O_2 decomposition (Fig. 3 SI) and CL oxidation, but the oxidant is consumed more effectively – only eightfold excess is required for CL oxidation. There is also no inhibition effect of intermediates on the activity of the amorphous sample and CL mineralization reaches the same value as over the Fe-silicalite-1 microcrystals.

Conclusions

A number of heterogeneous Fenton-type catalysts based on Fe-containing silicalite-1 and SiO_2 with different crystallinity and texture have been synthesized and tested in adsorption and wet hydrogen peroxide oxidation of phenol and clarithromycin lactobionate. IR spectroscopy enabled to estimate the crystallinity of the roentgen-amorphous sample by availability of the strong band at 550–562 cm^{-1}, attributed to double rings of tetrahedra in zeolitic framework. The splitting of the band around 1105 cm^{-1} in IR spectra with the formation of a band at 1032 cm^{-1} is probably associating with the difference between bulk and surface Si-O-Si modes and can be used to estimate the size of primary particles in the bulk of materials.

Crystallinity, texture and acidity of Fe-containing materials effect on the adsorption of phenol. Adsorption of phenol is monolayer on Fe-silicalite-1 samples and multilayer on samples containing amorphous phase mainly due to the surface defectiveness of last mentioned. Lower acidity of Fe-containing samples is more favorable for the adsorption of phenol being a weak

acid and the reaction between ferric sites and phenol with the formation of iron-phenolate complexes.

Inhibition effect of intermediates on the catalytic activity was observed for all Fe-containing samples under phenol oxidation by hydrogen peroxide, however there is no one in CL oxidation probably due to the absence of iron complexing agents among them. Active sites of crystalline sample are more stable for blocking by intermediates, apparently resulting from the protective function of zeolite framework. Sulphur-containing species on the surface of the materials, produced with the use of polystyrene templates, inhibit phenol oxidation inducing a long initial induction period. The decrease of Fe-silicalite-1 crystal size results in the better access of organic substrates to active oxidative particles, enabling the higher mineralization, especially of large molecules. Amorphous Fe-SiO_2 without sulfur admixtures was characterized by the most effective oxidant consumption in the oxidation of clarithromycin lactobionate despite of lower catalytic activity compared with crystallized samples.

Acknowledgments

The authors thank A.V. Polukhin for his help in carrying out catalytic experiments and N.A. Rudina for SEM analyses. This work from Russian side was conducted within the framework of State contract with Ministry of Education and Science if the Russian Federation No. 14.604.21.0159. The authors from Spanish side thank the Spanish Ministry of Economy and Competitiveness (MINECO), Generalitat Valenciana and FEDER (CTQ2015-66080-R MINECO/FEDER and PROMETEOII/2014/010) for financial support. J.G.A. thanks the Spanish Ministry of Economy and Competitiveness (MINECO) for his fellowship (BES-2013-063678).

All figures have the following color identification:

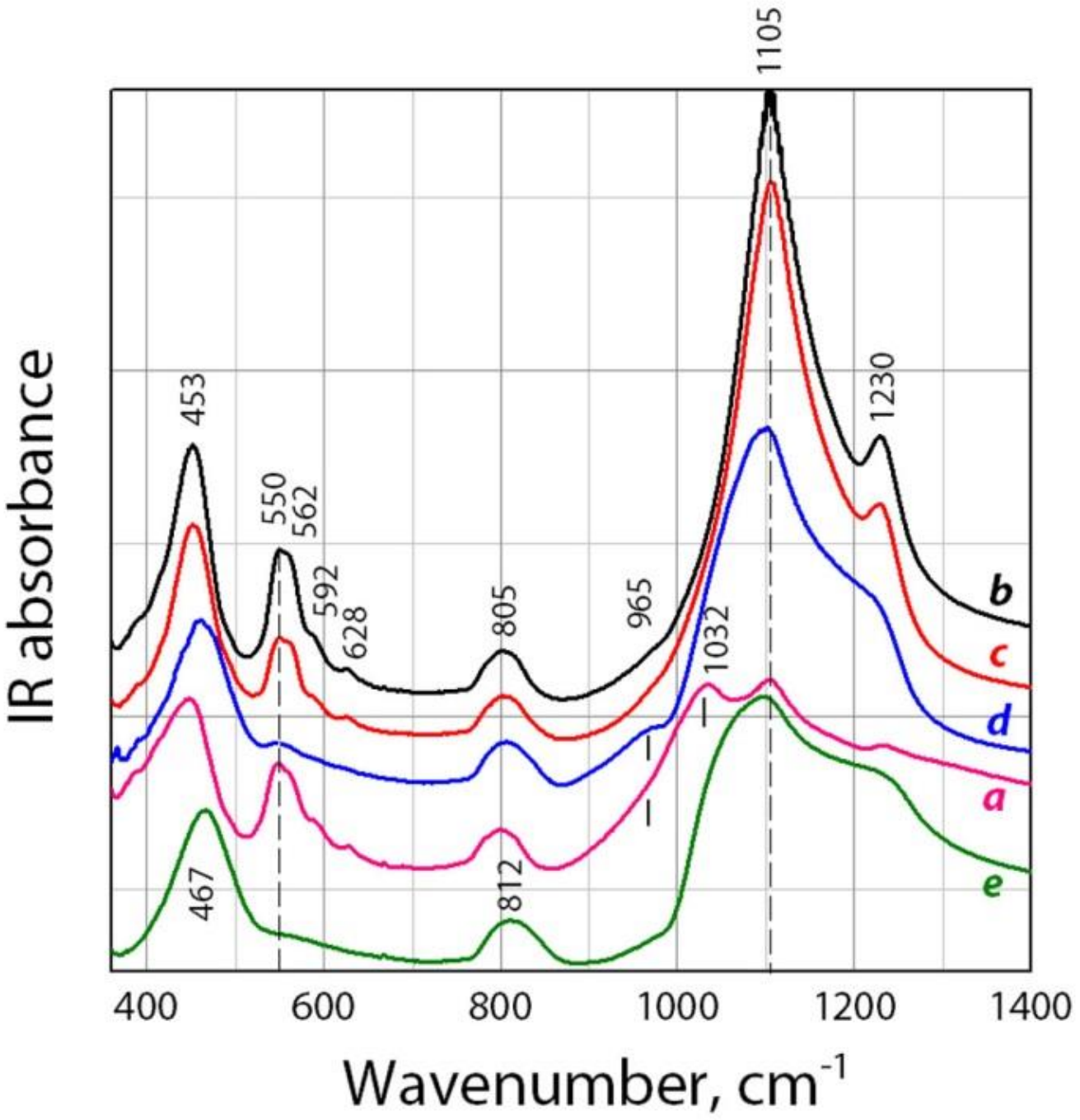

Fig. 1. IR spectra of KBr-diluted wafer of Fe-silicalite-1 microcrystals (a); Fe-silicalite-1 nanocrystals (b); Fe-composite (c); Fe-SiO_2 sample 1 (d); Fe-SiO_2 sample 2 (e).

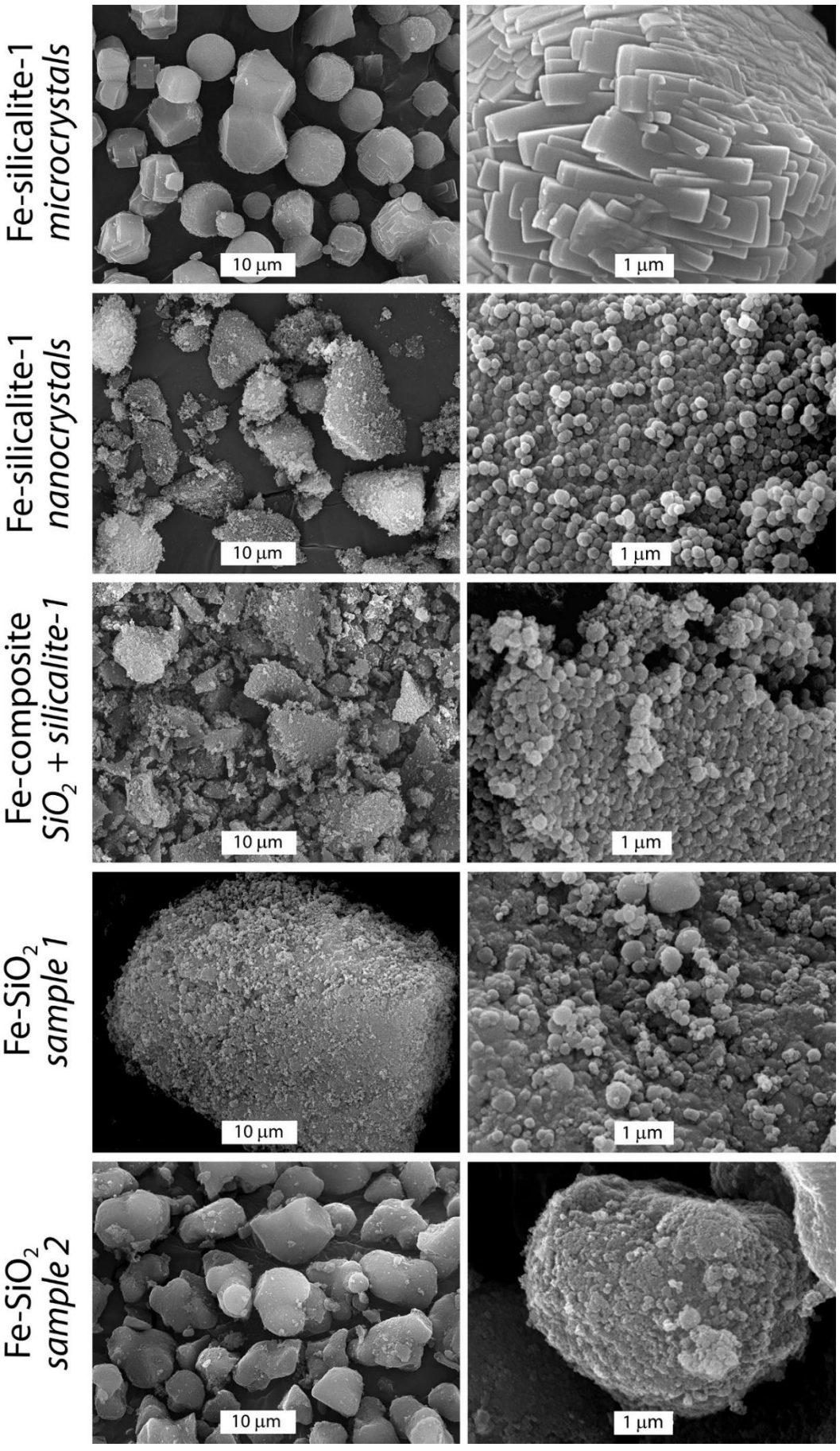

Fig. 2. SEM images of Fe-containing samples.

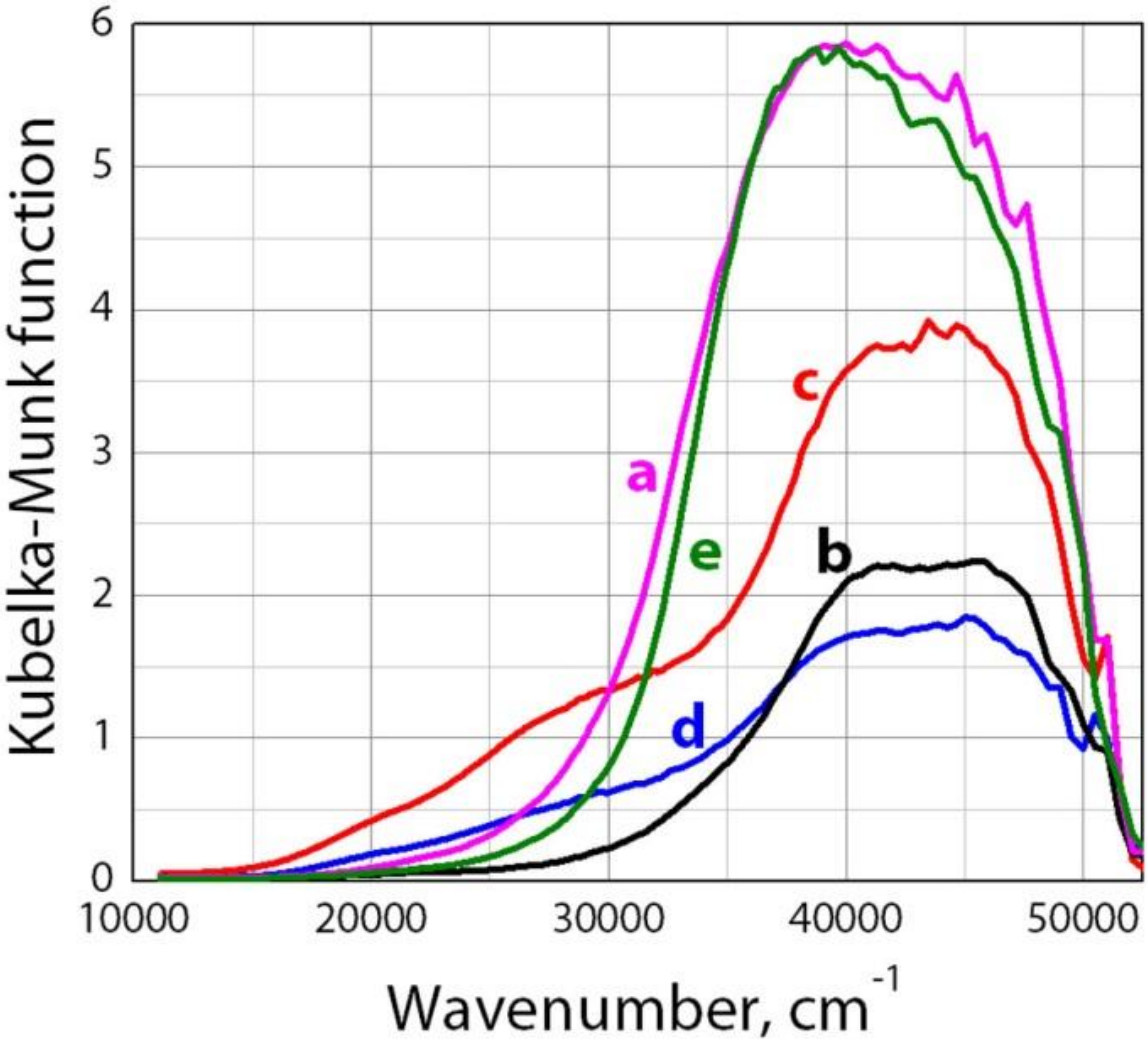

Fig. 3. UV-vis DR spectra of the Fe-containing samples: Fe-silicalite-1 microcrystals (a);Fe-silicalite-1 nanocrystals (b); Fe-composite (c); Fe-SiO_2 sample 1 (d); Fe-SiO_2 sample 2 (e).

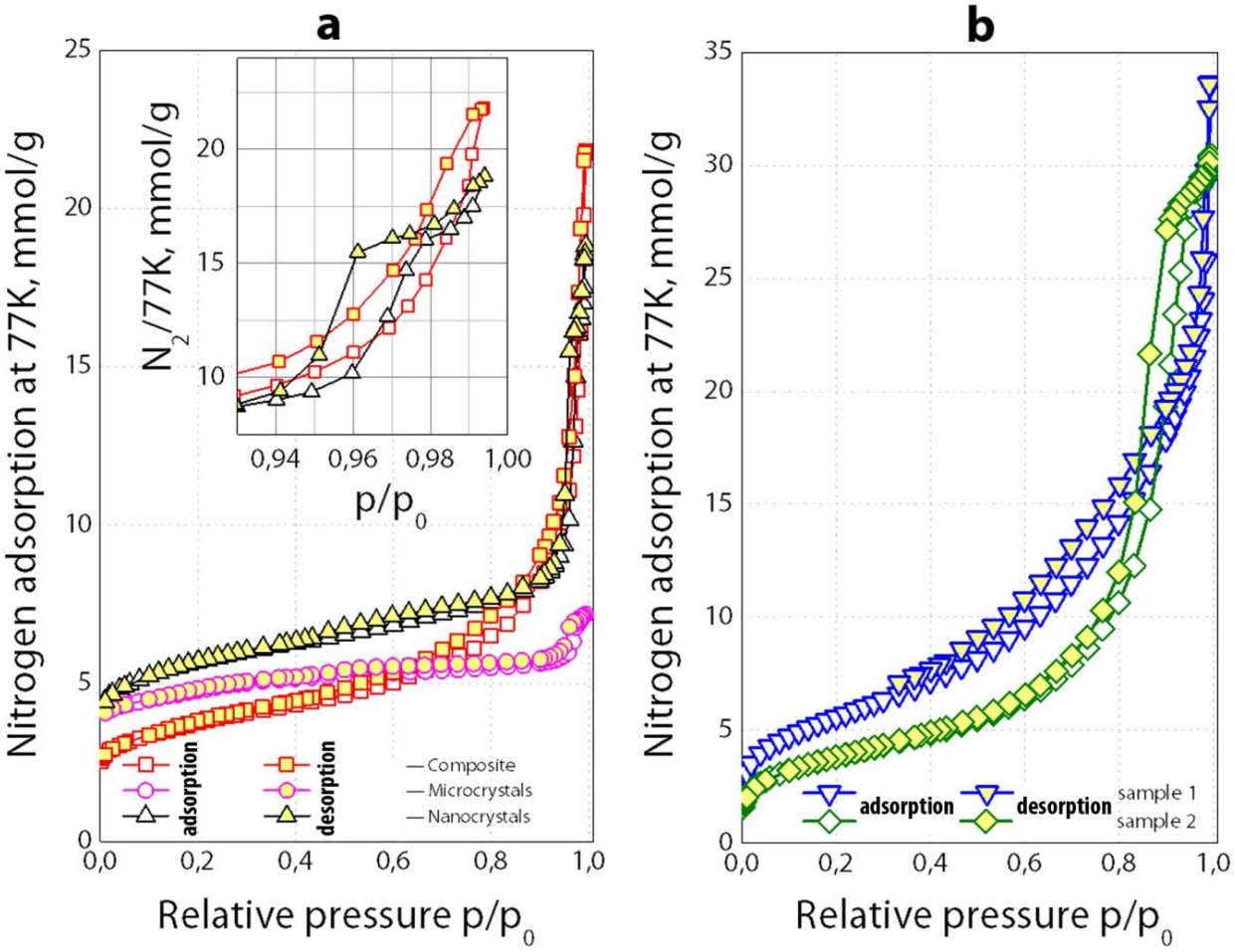

Fig.4. Isotherms of nitrogen adsorption at 77 K on Fe-containing samples with crystalline phase of silicalite-1 (a), and amorphous samples (b).

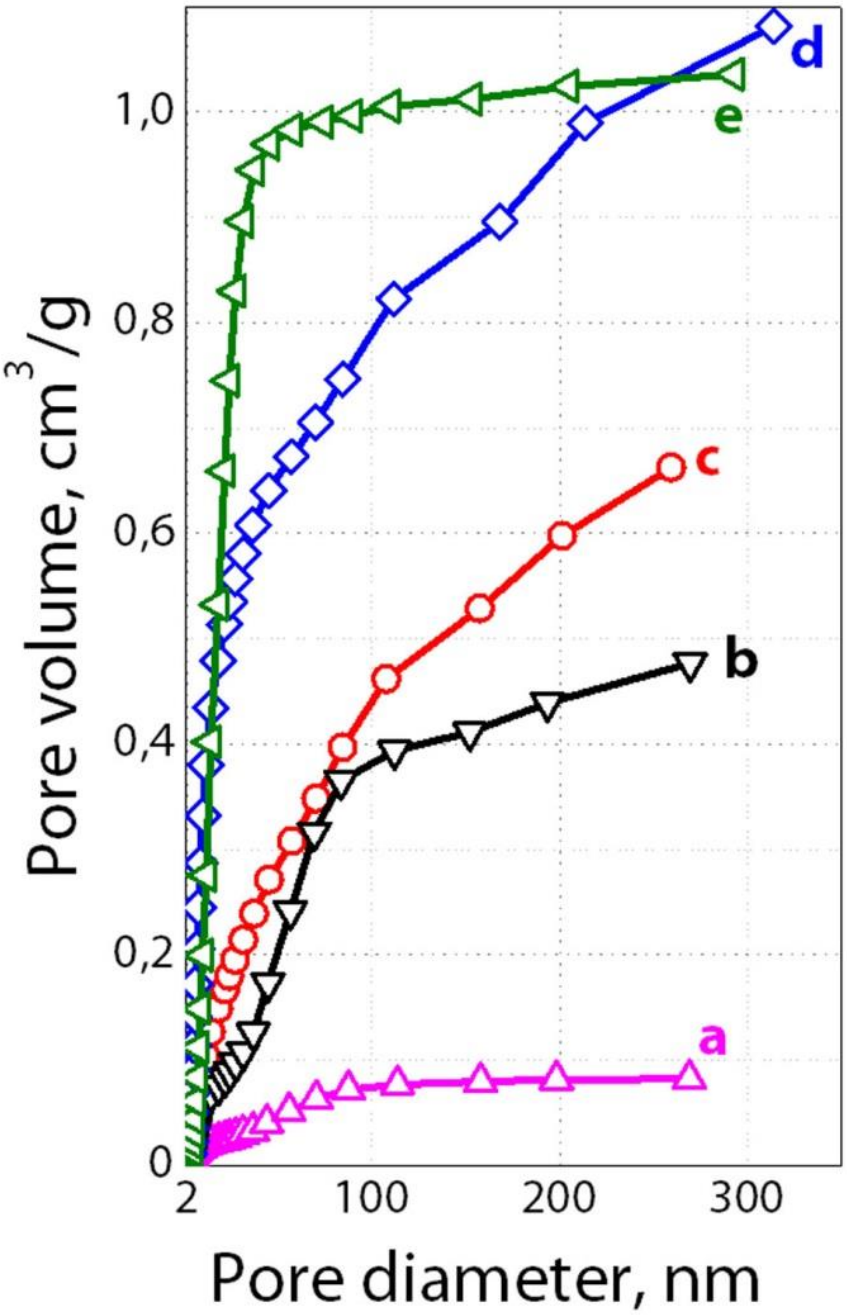

Fig. 5. Cumulative pore size distribution (BJH, adsorption branch) in Fe-containing samples: Fe-silicalite-1 microcrystals (a); Fe-silicalite-1 nanocrystals (b); Fe-composite (c); Fe-SiO_2 sample 1 (d); Fe-SiO_2 sample 2 (e).

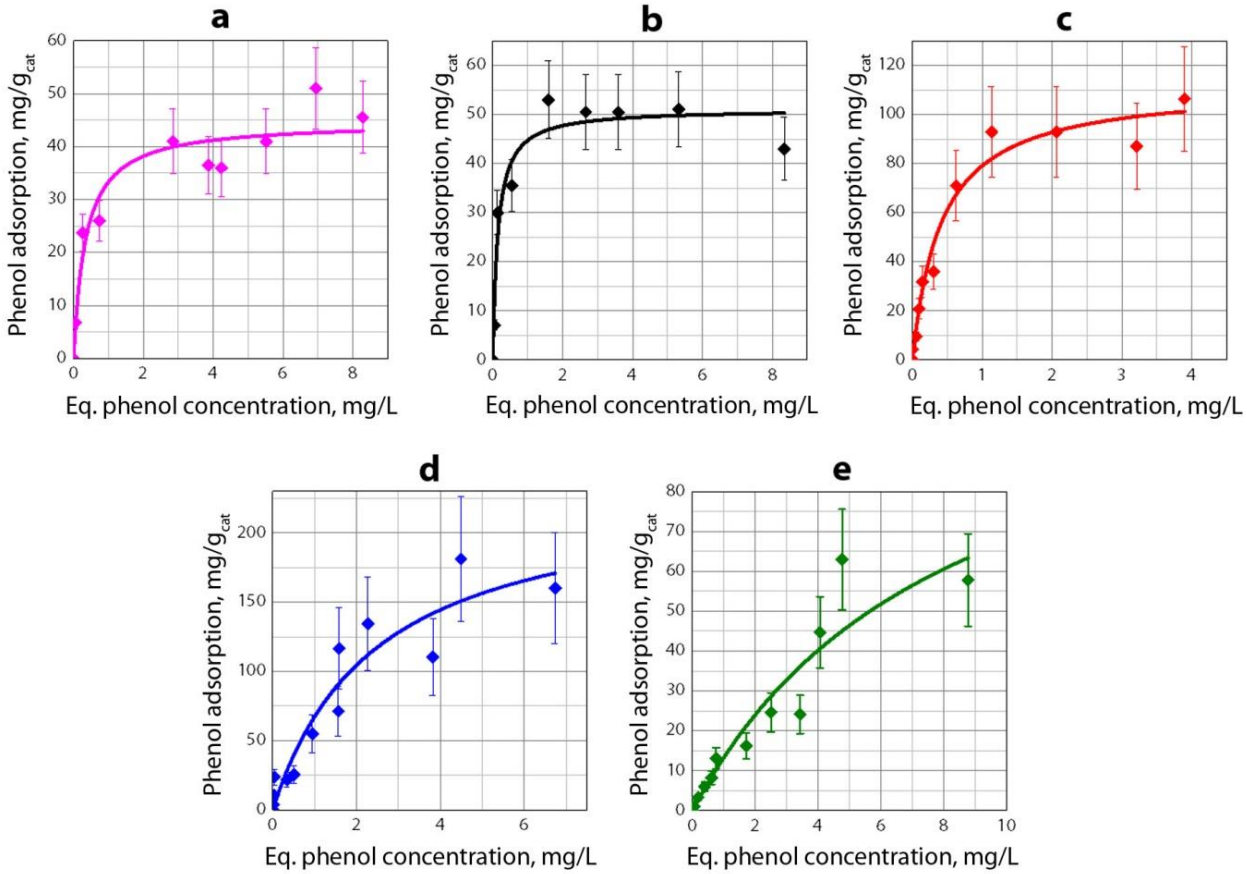

Fig. 6. Isotherms of phenol adsorption on Fe-containing samples: Fe-containing samples: Fe-silicalite-1 microcrystals (a); Fe-silicalite-1 nanocrystals (b); Fe-composite (c); Fe-SiO_2 sample 1 (d); Fe-SiO_2 sample 2 (e). Symbols – experimental data, lines – Langmuir model.

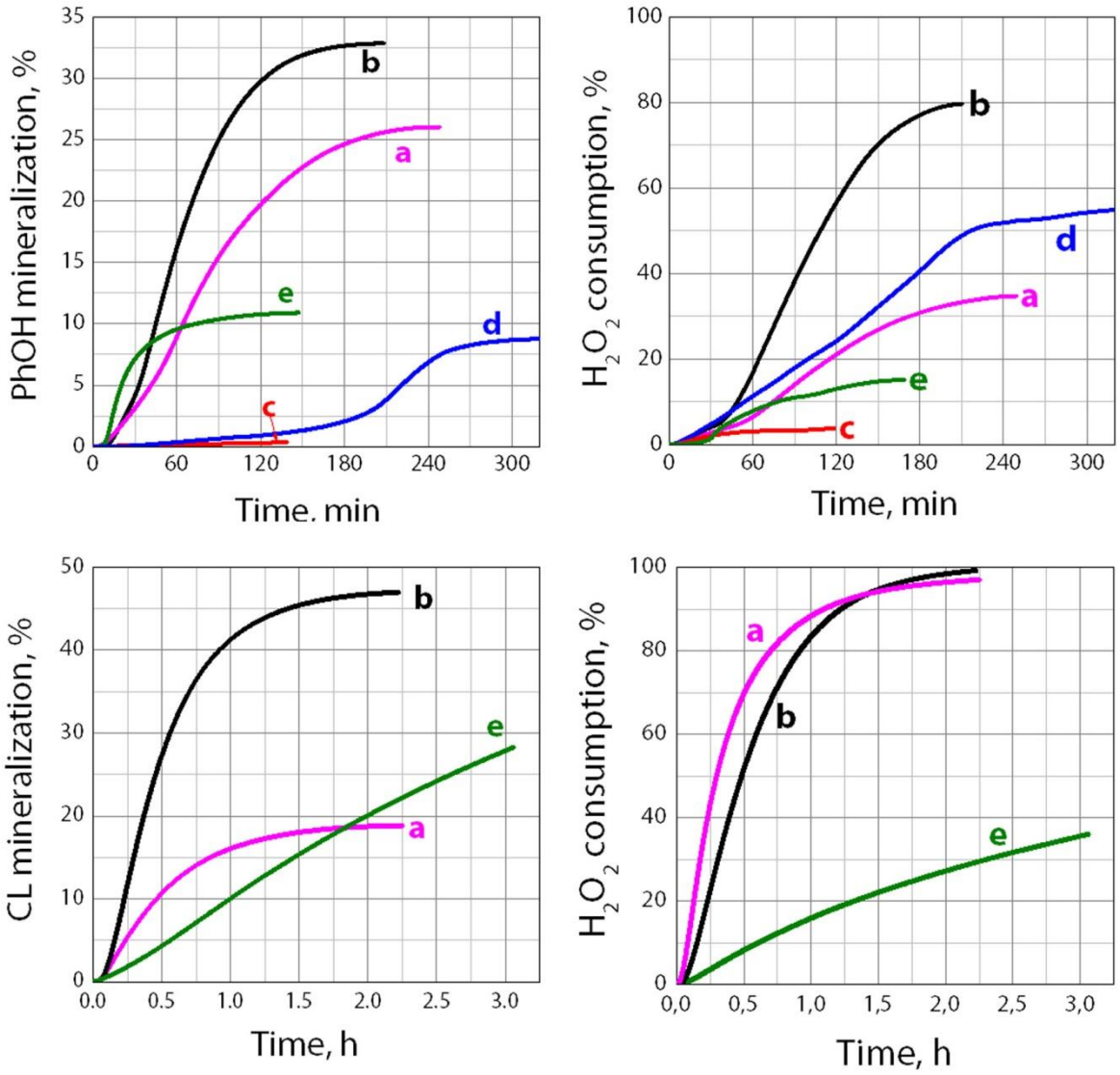

Fig. 7. Kinetic curves of phenol (upper) and CL (bottom) oxidation by H_2O_2 over Fe-containing samples according to CO_2 (left) and O_2 (right) evolving: Fe-silicalite-1 microcrystals (a);Fe-silicalite-1 nanocrystals (b); Fe-composite (c); Fe-SiO_2 sample 1 (d); Fe-SiO_2 sample 2 (e).

Experimental conditions: for phenol – $[H_2O_2]_0$ = 1 M, $[PhOH]_0$ = 0.5 g/L, [cat] = 20 g/L, T = 30 °C, for CL – $[H_2O_2]_0$ = 1.5 M, $[CL]_0$ = 0.3 g/L, [cat] = 20 g/L, T = 40 °C

Table 1. Crystallinity according to XRD and IR, and textural properties of iron-containing samples

Sample	Crystallinity, %		S_{BET}, m^2/g	S_{Ext}, m^2/g	V_{meso}, cm^3/g	V_{mic}, cm^3/g
	XRD	IR				
Fe-silicalite-1 microcrystals	97	68	402	133	0.08	0.11
Fe-silicalite-1 nanocrystals	100	100	463	223	0.48	0.10
Fe-composite	58	56	298	205	0.66	0.04
Fe-SiO_2 sample 1	0	6	448	456	1.07	0.0
Fe-SiO_2 sample 2	0	0	309	312	1.00	0.0

Table 2. Chemical composition and acidity according to TPD of NH_3 of iron-containing samples

Sample	Fe, wt.% ICP	Si, wt.% XFS	Al, wt.% XFS	Si/Al, mole/mole	S, wt.% XFS	NH_3 adsorption capacity, mmole/g
Fe-silicalite-1 microcrystals	1.95	65.8	0.11	574	-	0.52
Fe-silicalite-1 nanocrystals	1.28	67.9	0.07	931	-	0.23
Fe-composite	1.29	60.5	0.22	264	0.28	0.12
Fe-SiO_2 sample 1	1.89	58.6	0.12	468	-	0.12
Fe-SiO_2 sample 2	0.6	60.5	0.18	323	-	0.19

Table 3. Adsorption constant (K) and adsorption capacity (a_∞) according to Langmuir model of phenol adsorption, maximum adsorption capacity (a_{max}), that was experimentally observed, for Fe-containing samples

Sample	K, L/g	a_∞, mg/g_{cat}	a_{max}, mg/g_{cat}	$S_{PhOH}/S_{БЭТ}\cdot 100$, %		PhOH/Fe, at./at.
				model	experiment	
Fe-silicalite-1 microcrystals	2.9±0,7	45±3	50	33	36	1,5
Fe-silicalite-1 nanocrystals	7.0±1,4	50±3	50	32	31	2,3
Fe-composite SiO_2	2.5±0,5	110±6	100	108	97	4,6
Fe-SiO_2 sample-1	2.5±0,2	235±40	150	150	97	4,7
Fe-SiO_2 sample-2	0.12±0,07	120±50	60	114	56	5,9

Table 4. Catalytic characteristics for Fe-containing samples in wet peroxide oxidation of phenol (PhOH) and clarithromycin lactobionate (CL)

Sample	2 h-mineralization, %		H_2O_2 consumption, %		$\frac{H_2O_2 \text{ consumed}}{H_2O_2 \text{ stoichiom.}}$		$W_{max}(CO_2)$, mcg/s		$W_{max}(O_2)$, mcg/s	
	PhOH	CL	PhOH	CL	PhOH	CL	PhOH	CL	PhOH	CL
Fe-silicalite-1 microcrystals	20	19	21	97	14	21	0.64	0.95	6.7	0.3
Fe-silicalite-1 nanocrystals	29	47	56	98	26	21	1.14	2.50	21.3	0.2
Fe-composite SiO_2	1	n.d.	4	n.d.	54	n.d.	0.01	n.d.	2.7	n.d.
Fe-SiO_2 sample-1	<1	n.d.	24	n.d.	806	n.d.	0.02	n.d.	6.2	n.d.
Fe-SiO_2 sample-2	11	20	12	27	15	8	1.23	0.40	12.2	0.02

1 Autenrieth R L, Bonner J S, Akgerman A, Okaygun M, McCreary E M. Biodegradation of phenolic watstes. Journal of Hazardous Materials, 1991, 28(1–2): 29–53
2 Stich H F. The beneficial and hazardous effects of simple phenolic compounds. Mutation Research, 1991, 259(3–4): 307–324
3 Mohammadi S, Kargari A, Sanaeepur H, Abbassian K, Najafi A, Mofarrah E. Phenol removal from industrial wastewaters: a short review. Desalination and Water Treatment, 2014, 53(8): 2215–2234
4 Zhou L, Cao H, Descorme C, Xie Y, Phenolic compounds removal by wet air oxidation based processes, Front. Environ. Sci. Eng. 2018, 12(1): 1-20
5 S. Ahmed, M.G. Rasul, W.N. Martens, R. Brown, M.A. Hashib, Desalination 261 (2010) 3–18.
6 J. Jiang, H. Wang, X. Chen, S. Li, T. Xie, D. Wang, Y. Lin, J Colloid Interf Sci. 494 (2017) 130–138.
7 Y. Park, G.A. Ayoko, E. Horváth, R. Kurdi, J. Kristof, R.L. Frost, J Colloid Interf Sci. 393 (2013) 319–334.
8 S. Omwoma, C.T. Gore, Y.C. Ji, C.W. Hu, Y.F. Song Environmentally benign polyoxometalate materials Coord. Chem. Rev., 286 (2015), pp. 17-29
9 E.neyens, J. Baeyens. A review of classic Fenton's peroxidation as an advanced oxidation technique. Journal of Hazardous Materials B98 (2003) 33-50.
10 J. J. Pignatello, E. Oliveros, A. MacKay. Advanced oxidation processes for organic contaminant destruction based on the Fenton reaction and related chemistry. Critical Reviews in Environmental Science and Technology 36 (2006) 1-84.
11 D.J. Yin, L.Z. Zhang, X.F. Zhao, H. Chen, Q. Zhai Iron-glutamate-silicotungstate ternary complex as highly active heterogeneous Fenton-like catalyst for 4-chlorophenol degradation Chin. J. Catal., 36 (2015), pp. 2203-2210
12 S. Navalon, M. Alvaro, H. Garcia. Heterogeneous Fenton catalysts based on clays, silicas and zeolites. Applied Catalysis B: Environmental 99 (2010) 1-26.
13 C. Trellu, E. Mousset, Y. Pechaud, D. Huguenot, E.D. van Hullebusch, G. Esposito, M.A. Oturan Removal of hydrophobic organic pollutants from soil washing/flushing solutions: a critical review J. Hazard. Mater., 306 (2015), pp. 149-174
14 E.G. garrido-Ramirez, B.K.G. Theng, M.L. Mora. Clays and oxide minerals as catalysts and nanocatalysts in Fenton-like reactions – A review. Applied Clay Science 47 (2010) 182-192.
15 L. Cano-Casanova, A. Amorós-Pérez, M.Ouzzine, M.A.Lillo-Ródenas, M.C.Román-Martínez, One step hydrothermal synthesis of TiO_2 with variable HCl concentration: Detailed characterization and photocatalytic activity in propene oxidation, Applied Catalysis B: Environmental 220 (2018) 645–653
16 J. García-Aguilar, I. Miguel-García, J. Juan-Juan, I. Such-Basáñez, E. San Fabián, D. Cazorla-Amorós , Á. Berenguer-Murcia, Journal of Catalysis 338 (2016) 154–167
17 Jaime García-Aguilar, Diego Cazorla-Amorós, Ángel Berenguer-Murcia, Applied Catalysis A: General 538 (2017) 139–147
18 Kuznetsova, E.V., Savinov, E.N., Vostrikova, L.A., Parmon, V.N. Appl. Catal., B: Environ. (2004) 51/3, 165-170.
19 Makhotkina, O.A., Preis, S.V., Parkhomchuk, E.V. Appl. Catal., B: Environ. (2008) 84, 821–826.
20 Sashkina, K.A., Labko, V.S., Rudina, N.A., Parmon, V.N., Parkhomchuk, E.V. J. Catal. (2013) 299, 44–52.
21 Sashkina K. A., Parkhomchuk E. V., Rudina N. A., Parmon V. N. Microporous Mesoporous Mater. (2014) 189, 181–188.

22 F. Martínez, G. Calleja, J.A. Melero, R. Molina. Heterogeneous photo-Fenton degradation of phenolic aqueous solutions over iron-containing SBA-15 catalyst. Applied catalysis B: Environmental 60 (2005) 181-190.
23 F. Martinez, R. Molina, M.I. pariente, J.A. Siles, J.A. Melero. Low-cost Fe/SiO_2 catalysts for continuous Fenton processes. Catalysis Today 280 (2017) 176-183.
24 I.Mazilu, C. Ciotonea, A. Chirieac, B. dragoi, C. Catrinescu, A. Ungureanu, S. Petit, S. Royer, E. Dumitriu. Synthesis of highly dispersed iron species within mesoporous SBA-15 silica as efficient heterogeneous Fenton-type catalysts. Microporous and Mesoporous Materials 241 (2017) 326-337.
25 E.V.Parkhomchuk, V.S.Semeykina,K.A.Sashkina, A.G.Okunev, A.I.Lysikov, V.N. Parmon. Synthesis of Polystyrene Beads for Hard-Templating of Three-Dimensionally Ordered Macroporosity and Hierarchical Texture of Adsorbents and Catalysts, Topics in Catalysis, 2016 V. 60, Is.1, pp 178–189.
26 Thommes, M., Kaneko, K., Neimark, A. V., Olivier, J. P., Rodriguez-Reinoso, F., Rouquerol, J., & Sing, K. S. (2015). Physisorption of gases, with special reference to the evaluation of surface area and pore size distribution (IUPAC Technical Report). *Pure and Applied Chemistry*, *87*(9-10), 1051-1069.
27 Rouquerol, J., Rouquerol, F., Llewellyn, P., Maurin, G., & Sing, K. S. (2013). Adsorption by powders and porous solids: principles, methodology and applications. Academic press.
28 M.M.J. Treacy, J.B. Higgins, R. Ballmoos, Collection of Simulated XRD Powder Patterns for Zeolites, published by, Third revised edition, The Commission of the International Zeolite Association, 1996.
29 Standard test method for determination of relative crystallinity of zeolite ZSM-5 by X-Ray diffraction. ASTM International, D 5758-01.
30 T. Armaroli, L.J. Simon, M. Digne, T. Montanari, M. Bevilacqua, V. Valtchev, J. Patarin , G. Busca Effects of crystal size and Si/Al ratio on the surface properties of H-ZSM-5 zeolites // Applied Catalysis A: General 306 (2006) 78–84
31 G. Coudurier, C. Naccache, J.C. Vedrine, Uses of I.R. Spectroscopy in identifying ZSM Zeolite Structure. J Chem. Soc., Chem. Commun. (1982) 1413-1415
32 P.K. Dutta, K. Modana Rao, J.Y. Park, Correlation of Raman Spectra of Zeolites with Framework Architecture. J. Phys. Chem. 95 (1991) 6654-6656.
33 P.Ratnasamy, R. Kumar. Ferrisilicate analogs of zeolites. Catalysis Today (1991) 9, 4, 329-416.
34 Hensen, E. J. M., Zhu, Q., Hendrix, M. M. R. M., Overweg, A. R., Kooyman, P. J., Sychev, M. V., Santen, R. A.. J. Catal. 221 (2004) 2, 560-574.
35 Sashkina K. A., Parkhomchuk E. V., Rudina N. A., Parmon V. N. The role of zeolite FeZSM-5 porous structure for heterogeneous Fenton catalyst activity and stability. *Microporous & Mesoporous Materials*, Volume 189, 1 May 2014, Pages 181–188.
36 J.S. Mattson, H.B. Mark JR., M.D. Malbin, W.J. Weber JR., J.C. Crittenden. Surface chemistry of active carbon: specific adsorption of phenols. Journal of Colloid and Interface Science 31, 1 (1969) 116-130.